

# Switching-loss reduction technique in active power filters without auxiliary circuits

ISSN 1755-4535

Received on 12th November 2014

Revised on 20th July 2015

Accepted on 27th August 2015

doi: 10.1049/iet-pel.2014.0864

www.ietdl.org

Chi-Seng Lam<sup>1,2</sup> ✉, Man-Chung Wong<sup>1,2</sup>, Ning-Yi Dai<sup>2</sup>, Wai-Hei Choi<sup>2</sup>, Xiao-Xi Cui<sup>2</sup>,  
 Chi-Yung Chung<sup>3</sup>

<sup>1</sup>State Key Laboratory of Analog and Mixed-Signal VLSI, University of Macau, Macao, People's Republic of China

<sup>2</sup>Department of Electrical and Computer Engineering, Faculty of Science and Technology, University of Macau, Macao, People's Republic of China

<sup>3</sup>Department of Electrical and Computer Engineering, University of Saskatchewan, Saskatoon, Saskatchewan, Canada

✉ E-mail: C.S.Lam@iee.org

**Abstract:** To reduce the active power filter (APF) system switching loss, the usual method is to apply different soft-switching techniques. However, this would increase the system initial cost. In this study, a switching loss and switching noise reduction control strategy for APF under reactive power and current harmonics compensation is proposed, which can be applied to the existing APF systems in worldwide, thus causing economic benefits. The minimum dc-link operating voltage of APF is computed through both fundamental and harmonic frequencies analysis. Then an adaptive dc-link voltage controller for the APF is proposed, such that the compensating range of the APF is adaptively varied according to the variation of the loading. Thus, the switching loss and switching noise of the APF can be lowered. Moreover, the design criteria of the proportional and integral gains of the adaptive dc voltage controller are presented and discussed. Finally, simulation and experimental results of a 110 V, 5 kVA APF experimental prototype are given to prove the validity of the proposed control strategy for the APF in current quality compensation, and at the same time reducing switching loss and switching noise during operation.

## 1 Introduction

Traditionally, passive power filters (PPFs) have been considered as a good solution for current harmonics compensation and displacement power factor (PF) correction in distributed power systems [1–6] owing to their simplicity, low initial cost, etc. However, they have low dynamic performance, resonance problems, poor system robustness and so on [1–6], in which those disadvantages are not appreciated for customers. Active power filter (APF) concept was first proposed by L. Gyugyi in 1976 [2], since then the APFs were rapidly developed. APFs can solve those problems existing in PPFs, but they have high rating with high initial cost limitation. Moreover, they need to bear a relative high switching loss and switching noise during operation. Conventionally, all APFs are being operated at a high constant dc-link voltage level for ensuring the compensation performance [1, 3–11]. In addition, as many APFs have been installed and are operating in Japan and all around the world [12, 13], their operating switching loss is a notable application concern. For example, the presented APF operating switching loss is about 7–9% at its 60% rated power [14] and 3–5% at its full rated power [15–17], which is a significant power loss. To reduce the APF system switching loss, the usual method is to apply soft-switching techniques. Table 1 summarises the comparison among different soft-switching circuits [18–20]: actively clamped resonant dc-link (ACRDCL) [19], auxiliary resonant commutated pole (ARCP) [19, 20] and negative-bus auxiliary resonant circuit (NBARC) [18]. From Table 1, even though they can significantly reduce the APF inverter power loss, it is obvious that applying soft-switching techniques would increase the APF system initial cost because it requires extra switching devices, passive elements and so on. To increase the value proposition of the APF without changing its structure or design [21], it would be a good approach if its switching loss can be reduced by further developing the control algorithm for the existing APF systems. As the switching loss is

directly proportional to the inverter voltage in dc side [22], a higher switching loss will be induced when the APF is being operated at a high dc-link voltage, and vice versa. Therefore, if the dc-link voltage can be varied according to different loading situations, the APF can obtain better performances and also reduce switching loss. However, the adaptive dc voltage control strategy for APF is still lack of investigation and study.

In [23], parameter design procedures for minimum dc-link voltage operation of hybrid power-quality compensator (HPQC) in high-speed co-phase traction power supply system are proposed. The HPQC is composed of two single-phase converters connected back-to-back and sharing the same dc-link capacitor for energy exchange. One of the converters is connected to two phases of the three-phase power system through coupling inductors (L coupling) and single phase V/V transformer, while the other one is connected to them through coupling capacitor and inductor (LC coupling) and single-phase V/V transformer. However, this work does not present any dc-link voltage control strategy for HPQC and just provides an extra dc voltage source for performing simulations and experiments. To reduce the switching loss and switching noise for the hybrid active power filter (HAPF) Lam *et al.* [24] proposed an adaptive dc-link voltage control strategy for three-phase HAPF reactive power compensation only, but the proposed strategy does not include current harmonic consideration. In [25], the minimum dc-link voltage deduction for HAPF without and with coupling neutral inductor is proposed, and the advantages of adding neutral inductor are also discussed. However, the dc voltage control strategy is not being discussed in [25]. On the basis of the works presented in [24, 25], Lam *et al.* [26] develop and integrate the adaptive dc voltage control strategy [24] and the addition of coupling neutral inductor [25] into the HAPF in both dynamic reactive power and current harmonics compensation, in which the switching loss and switching noise can be greatly reduced. After the development of adaptive dc voltage control for HAPF [24–26], it proves that the adaptive control strategy can

**Table 1** Comparison among different soft-switching circuits [18–20]

Auxiliary circuit items	ACRDCL	ARCP	NBARC
no. of switches	1	6	2
no. of diode	1	6	2
no. of capacitor	2	6	1
no. of inductor	1	3	1
peak voltage conducting losses	1.5–1.8 p.u. high	0.5 p.u. low	0.5 and 1 p.u. low
insertion and resonant bus point	positive dc-link	positive dc-link	negative dc-link
inverter loss reduction (compared with hard switching)	maximum: ~60% at 10 kHz, $V_{dc} = 300\text{ V}$ , $I_o = 100\text{ A}_{\text{peak}}$ [19]	maximum: ~40% at 18 kHz, $V_{dc} = 300\text{ V}$ , $I_o = 100\text{ A}_{\text{peak}}$ [19]	[18] (power device temp. decreased by 15 and 11% at 50 and 100% loading to reflect loss decrease)

bring benefits (switching loss and switching noise reduction) to the HAPF system during operation. In this paper, based on the effective results in [27], the adaptive dc voltage control idea is migrated into the APF to investigate its switching loss and switching noise reduction performances. So that this adaptive dc control strategy can also be applied to the existing APF systems in worldwide, thus causing some economic benefits.

Even though the adaptive dc voltage control strategy has been proposed in HAPF, the control algorithm cannot be simply and directly applied into APF. Therefore, it is necessary to do further research analysis and investigation, which is the motivation of this paper. Furthermore, the main contributions of this paper are:

- Deduce and analyse APF minimum dc-link voltage for reactive power and current harmonics compensation with the help of [27].
- Propose an adaptive dc-link voltage control strategy for APF reducing switching loss and noise, and improve compensation performance.
- Present and analyse the design criteria of the proportional and integral gains of the dc-link voltage controller.
- Present extensive simulation and experimental results for an 110 V, 5 kVA APF experimental prototype to validate the proposed control technique in comparison to the conventional method.

In this paper, a brief introduction of research background and motivation is covered in Section 1. In Section 2, a three-phase four-wire APF with its corresponding equivalent fundamental and harmonic circuit models are presented. According to its circuit models, the required minimum dc-link voltage can be calculated. Then, the adaptive dc-link voltage controller for the APF and also the design criteria of its proportional and integral gains are presented and discussed in Section 3. In Section 4, the parameters selection of the APF system, simulation verifications and experimental results obtained from hardware prototype are presented. Finally, a conclusion is given in Section 5. As this paper mainly focuses on the APF application in low-voltage power distribution side, the neutral wire is usually presented and the following analysis and discussion will only focus on inductive loads.

## 2 Three-phase four-wire APF required minimum dc-link voltage for reactive power and current harmonics compensation

The overall circuit diagram of the three-phase four-wire APF is illustrated in Fig. 1, where the subscript 'x' represents phases *a*, *b*, *c*, *n*.  $v_{sx}$  represents the source voltage,  $v_x$  represents the load voltage,  $L_s$  represents the system inductance.  $i_{sx}$ ,  $i_{Lx}$  and  $i_{cx}$  represent the source, load and inverter current.  $L_c$  represents the coupling inductor.  $C_{dc}$  is dc-link capacitor and the upper and

lower dc capacitor voltages are represented by  $V_{dcU}$  and  $V_{dcL}$  with  $V_{dcU} = V_{dcL} = 0.5V_{dc}$ .

The APF equivalent single-phase circuit models at fundamental and harmonic frequencies are shown in Fig. 2, where the subscripts '*f*' and '*n*' represent the fundamental and harmonic frequency components. And the active part of APF can be regarded as a controllable voltage source by pulse-width modulation (PWM) technique. All parameters for the following analysis are in root mean square (rms) values.

### 2.1 Required dc-link voltage at fundamental frequency

If  $v_{sx}$  and  $v_x$  as shown in Fig. 1 are pure sinusoidal without harmonic components,  $\underline{V}_{sx} = \underline{V}_x = \underline{V}_{x_f} = |\underline{V}_x| = V_x$ . From Fig. 2a, the voltage vector of APF inverter at fundamental frequency is expressed as

$$\underline{V}_{invx_f} = \underline{V}_x + \underline{Z}_{Lc_f} \cdot \underline{I}_{cx_f} \quad (1)$$

All vectors in (1) are in fundamental frequency, where the compensating current  $\underline{I}_{cx_f}$  is composed by  $\underline{I}_{cx_f} = \underline{I}_{cx_{fp}} + j\underline{I}_{cx_{fq}}$ . The subscripts '*p*' and '*q*', represent the active and reactive components, respectively.  $\underline{I}_{cx_{fp}}$  represents the fundamental active current for contributing the active power flow between the source and APF while  $\underline{I}_{cx_{fq}}$  represents the fundamental reactive current for compensating loading reactive power.  $\underline{V}_{invx_f}$  in (1) can also be rewritten as

$$\underline{V}_{invx_f} = \underline{V}_{invx_{fp}} + j\underline{V}_{invx_{fq}} \quad (2)$$

where

$$\underline{V}_{invx_{fp}} = \underline{V}_x - \underline{I}_{cx_{fp}} X_{Lc_f} \quad (3)$$

$$\underline{V}_{invx_{fq}} = \underline{I}_{cx_{fq}} X_{Lc_f}$$

From (3),  $\underline{I}_{cx_{fp}}$  and  $\underline{I}_{cx_{fq}}$  can be expressed as

$$\underline{I}_{cx_{fp}} = \frac{\underline{V}_{invx_{fq}}}{X_{Lc_f}} \quad (4)$$

$$\underline{I}_{cx_{fq}} = \frac{\underline{V}_x - \underline{V}_{invx_{fp}}}{X_{Lc_f}} \quad (5)$$

On the condition that the inverter dc voltage control is implemented, the steady-state  $\underline{I}_{cx_{fp}}$  from the inverter is small ( $\underline{I}_{cx_{fp}} \simeq 0$ ). For  $V_{dcU} = V_{dcL} = 0.5V_{dc}$  and modulation index  $m = 1$ ,  $R_{V_{dc}}$  represents the ratio between  $V_{dcU}$ ,  $V_{dcL}$  and load voltage  $V_x$  reference to neutral *n* [24]

$$R_{V_{dc}} = \frac{\pm V_{invx_f}}{V_x} = \frac{\pm 0.5V_{dc}/\sqrt{2}}{V_x} = \pm \frac{V_{dc}}{2\sqrt{2}V_x} \quad (6)$$

where  $V_{invx_f}$  is the inverter fundamental voltage in rms value.

As the active fundamental current  $\underline{I}_{cx_{fp}}$  is assumed to be very small ( $\underline{I}_{cx_{fp}} \simeq 0$ ) at steady state, the APF injects pure fundamental reactive current, the reactive power ( $Q_{cx_f}$ ) provided by the APF can be computed as

$$Q_{cx_f} = \text{Im}(\underline{V}_x \underline{I}_{cx_f}^*) = -V_x \underline{I}_{cx_{fq}} = -Q_{cx_f, Lc} (1 - R_{V_{dc}}) \quad (7)$$

where  $Q_{cx_f, Lc} = (V_x^2 / X_{Lc_f}) > 0$ , which is the reactive power provided by the coupling inductor.

From Fig. 1, to achieve the source-side reactive power  $Q_{sx_f} = 0$ , the compensating reactive power should be equalled to the loading reactive power, that is  $Q_{cx_f} = Q_{Lx_f}$ . By setting  $Q_{cx_f} = Q_{Lx_f}$ , via (6) and (7), the required minimum dc voltage  $V_{dcx_f}$  for reactive power

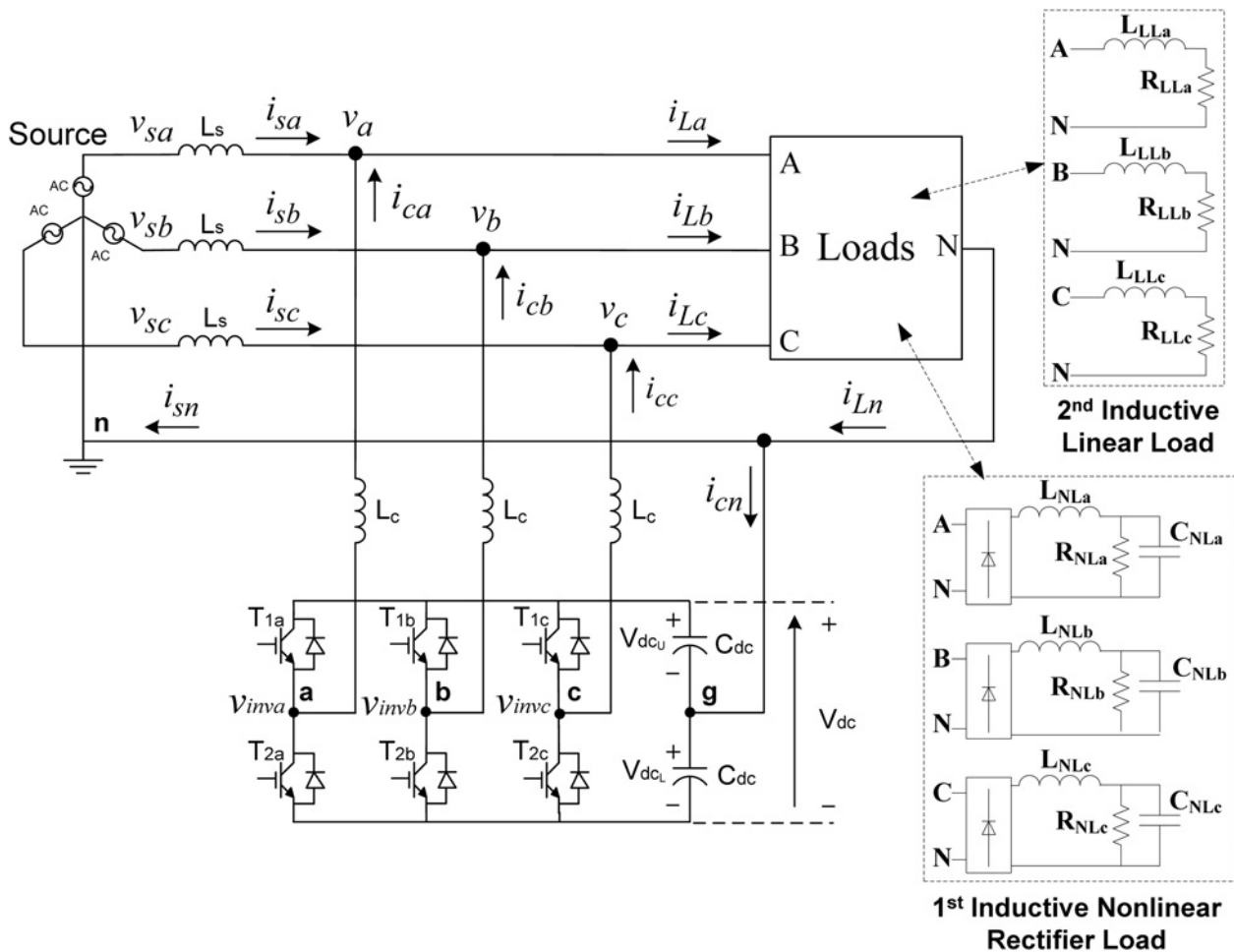


Fig. 1 Circuit structure of a three-phase four-wire APF

compensation in each phase can be found

$$V_{dcxf} = \sqrt{2}V_{invxf} = \sqrt{2} V_x \cdot N \quad (8)$$

where  $N = \left| 1 + \frac{Q_{Lxf}}{Q_{cxf-Lc}} \right|$ . Once  $Q_{Lxf}$  is calculated,  $V_{dcxf}$  in each phase can be obtained.

(i) For pure resistive load consideration: When the load is pure resistive, the loading reactive power  $Q_{Lxf} = 0$ ,  $N = 1$ . From (8), the required  $V_{dcxf} = 2\sqrt{2}V_x$ .

(ii) For inductive load consideration: When the load is inductive,  $Q_{Lxf} > 0$ ,  $N > 1$  as  $Q_{cxf-Lc} > 0$ . From (8), the required  $V_{dcxf} = 2\sqrt{2}V_x \cdot N > 2\sqrt{2}V_x$ .

(iii) For capacitive load consideration: When the load is capacitive,  $Q_{Lxf} < 0$ ,  $N \in \mathbb{R}$ . Thus, the required  $V_{dcxf} = 2\sqrt{2}V_x \cdot N$ . When  $Q_{Lxf} = -Q_{cxf-Lc}$ , the minimum dc-link voltage requirement ( $V_{dcxf} = 0$ ) can be achieved. Moreover,  $V_{dcxf}$  can be larger or smaller than  $2\sqrt{2}V_x$ , which depends on the sign of  $Q_{Lxf}$  and the values of  $Q_{Lxf}$  and  $Q_{cxf-Lc}$ .

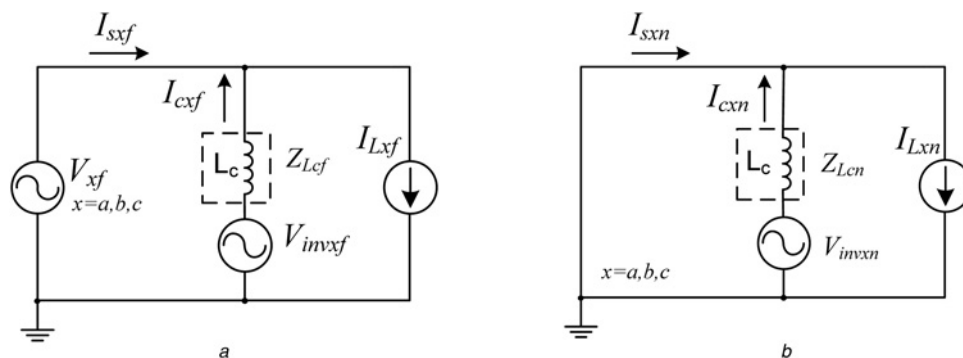


Fig. 2 APF equivalent single-phase circuit models at

- a Fundamental frequency
- b Harmonic frequency

**Table 2** Minimum dc-link voltage deduction steps of the APF

(1) Fundamental frequency	Minimum dc-link voltage for compensating reactive power:	(8)
	$V_{dcxf} = \sqrt{2}V_{invxf} = \sqrt{2}V_x \left  1 + \frac{Q_{Lx_f}}{Q_{cx_f-Lc}} \right $	
	where $Q_{Lx_f}$ is loading fundamental reactive power, $Q_{cx_f-Lc}$ is the reactive power provided by coupling $L_c$ .	
(2) Harmonic frequencies	Minimum dc-link voltage for compensating each $n$ th-order current harmonic:	(11)
	$V_{dcxn} = \sqrt{2}V_{invxn} = \sqrt{2} n\omega L_c  I_{cxn} $	
	where $ I_{cxn}  =  I_{Lxn} $ , $n = 2, 3, \dots, \infty$ , $\omega = 2\pi f$	
(3) All frequencies	Minimum dc-link voltage:	(13)
	$V_{dc\_min} = \max(2V_{dca}, 2V_{dcb}, 2V_{dcc})$	(12)
	Where $V_{dcx} = \sqrt{ V_{dcxf} ^2 + \sum_{n=2}^{\infty}  V_{dcxn} ^2}$ where $n = 2, 3, \dots, \infty$	

## 2.2 Required dc-link voltage at harmonic frequency

To compensate harmonic current generated by the non-linear load, APF should provide the corresponding harmonic output voltages  $V_{invxn}$ . According to Fig. 2b,  $V_{invxn}$  at each  $n$ th-order current harmonic can be expressed as

$$V_{invxn} = |n\omega L_c||I_{cxn}|, \quad n = 2, 3, \dots, \infty \quad (9)$$

where  $I_{cxn}$  represents the  $n$ th-order compensating current. When the APF is used to perform current harmonic compensation, the absolute  $I_{cxn}$  should be equal to

$$|I_{cxn}| = |I_{Lxn}| \quad (10)$$

where  $I_{Lxn}$  is the  $n$ th-order harmonic current of the loading. Thus, the required minimum dc-link voltage at each harmonic order  $V_{dcxn}$  for compensating the corresponding harmonic current can be found

$$V_{dcxn} = \sqrt{2}V_{invxn} = \sqrt{2}|n\omega L_c||I_{cxn}| \quad (11)$$

In the following, the APF final required dc-link voltage for both reactive power and current harmonics compensation will be presented and discussed.

## 2.3 Final required dc-link voltage

Combining the required dc-link voltage in both fundamental and harmonic circuits, the final dc-link voltage  $V_{dcx}$  can be computed by taking their rms value, thus,  $V_{dcx}$  can be expressed as

$$V_{dcx} = \sqrt{|V_{dcxf}|^2 + \sum_{n=2}^{\infty} |V_{dcxn}|^2} \quad (12)$$

Assumed that there are slight deviations among three-phase compensating currents of APF, thus there are three sets of minimum dc-link voltage value with respect to each phase parameter values. To guarantee the compensation performance of APF in each phase, the final required minimum dc-link voltage ( $V_{dc\_min}$ ) for the three-phase four-wire APF can be obtained by (13), where the calculated value by (13) is sufficient to compensate the reactive power and current harmonics problems for three phases. Table 2 summarises the minimum dc-link voltage

deduction steps of the three-phase four-wire APF, in which it has different  $V_{dcxf}$  and  $V_{dcxn}$  equations as compared with those of HAPF [24–26]

$$V_{dc\_min} = \max(2V_{dca}, 2V_{dcb}, 2V_{dcc}) \quad (13)$$

## 3 Adaptive dc-link voltage control strategy for a three-phase four-wire APF

In the following, the adaptive dc-link voltage control strategy is being applied to the three-phase four-wire APF system for lowering the operational switching loss and switching noise. The overall control block diagram is shown in Fig. 3, in which it consists of the following control blocks.

### 3.1 Instantaneous power compensation control block

The reference compensating currents for APF ( $i_{cx-q}$ ) are calculated by the three-phase instantaneous  $pq$  theory [28].

### 3.2 Adaptive dc-link voltage control block

The adaptive dc-link voltage control block is composed by three control algorithms: (i) computation of adaptive minimum dc-link voltage  $V_{dc\_min}$ , (ii) determination of final reference dc-link voltage level  $V_{dc}^*$  and (iii) proportional/proportional–integral (P/PI) control for dc-link voltage tracking.

(i) *Computation of adaptive minimum dc-link voltage ( $V_{dc\_min}$ ):* First of all, the loading instantaneous reactive power  $q_{Lxf}$  is obtained with the help of single-phase instantaneous  $pq$  theory [29] and low-pass filters with cut-off frequency  $f_{cut} = 5$  Hz. As  $-q_{Lxf}/2$  can usually keep as a constant value for one cycle or more, the loading fundamental reactive power consumption  $Q_{Lx_f}$  in each phase can be approximately treated as  $Q_{Lx_f} \approx -q_{Lxf}/2$ . The required  $V_{dcxf}$  for compensating each phase  $Q_{Lx_f}$  can be calculated by using (8). By using fast Fourier transform (FFT), the load current spectra  $|I_{Lxn}|$  up to the considered harmonic order  $n$  can be computed. Then, the required  $V_{dcxn}$  for compensating each  $n$ th-order harmonic can be calculated by using (11). Finally,  $V_{dc\_min}$  for the three-phase four-wire APF can be determined by (12) and (13).

(ii) *Determination of final reference dc-link voltage level ( $V_{dc}^*$ ):* The adaptive dc control strategy will vary the reference  $V_{dc}^*$  in reality, thus may cause a frequent dc voltage fluctuation, and deteriorate the APF performances [30]. To relax this,  $V_{dc}^*$  determination process proposed in [24] is applied.

(iii) *P/PI control for dc-link voltage tracking:* The adaptive dc voltage level for APF can be achieved by feedback dc voltage controlled signal as active current reference component ( $dc_p$ ) instead of both active and reactive current reference components of HAPF [24, 26, 31], the phenomenon can be explained with the help of [31]

$$dc_p = K_p \cdot (V_{dc}^* - V_{dc}) + K_I \int (V_{dc}^* - V_{dc}) dt \quad (14)$$

where  $dc_p$  aims to change and maintain the dc-link voltage level.  $K_p$  is the proportional gain, while  $K_I$  is the integral gain of the controller. With the help of the three-phase instantaneous  $pq$  theory [28] and  $dc_p$  term,  $V_{dc}$  can track its reference  $V_{dc}^*$  by varying the three-phase dc voltage control reference compensating currents  $i_{cx\_dc}$  in  $a-b-c$  coordinates. In the following, the design criteria for  $K_p$  and  $K_I$  will be discussed.

Fig. 4 shows the dc-link voltage control block diagram of APF, where  $V_{invxfp} = |V_x + |I_{cx}| |X_{Lc}|$  is the active component of inverter fundamental voltage,  $I_{cx\_fq}$  is fundamental reactive compensating current. When PI controller is applied, the

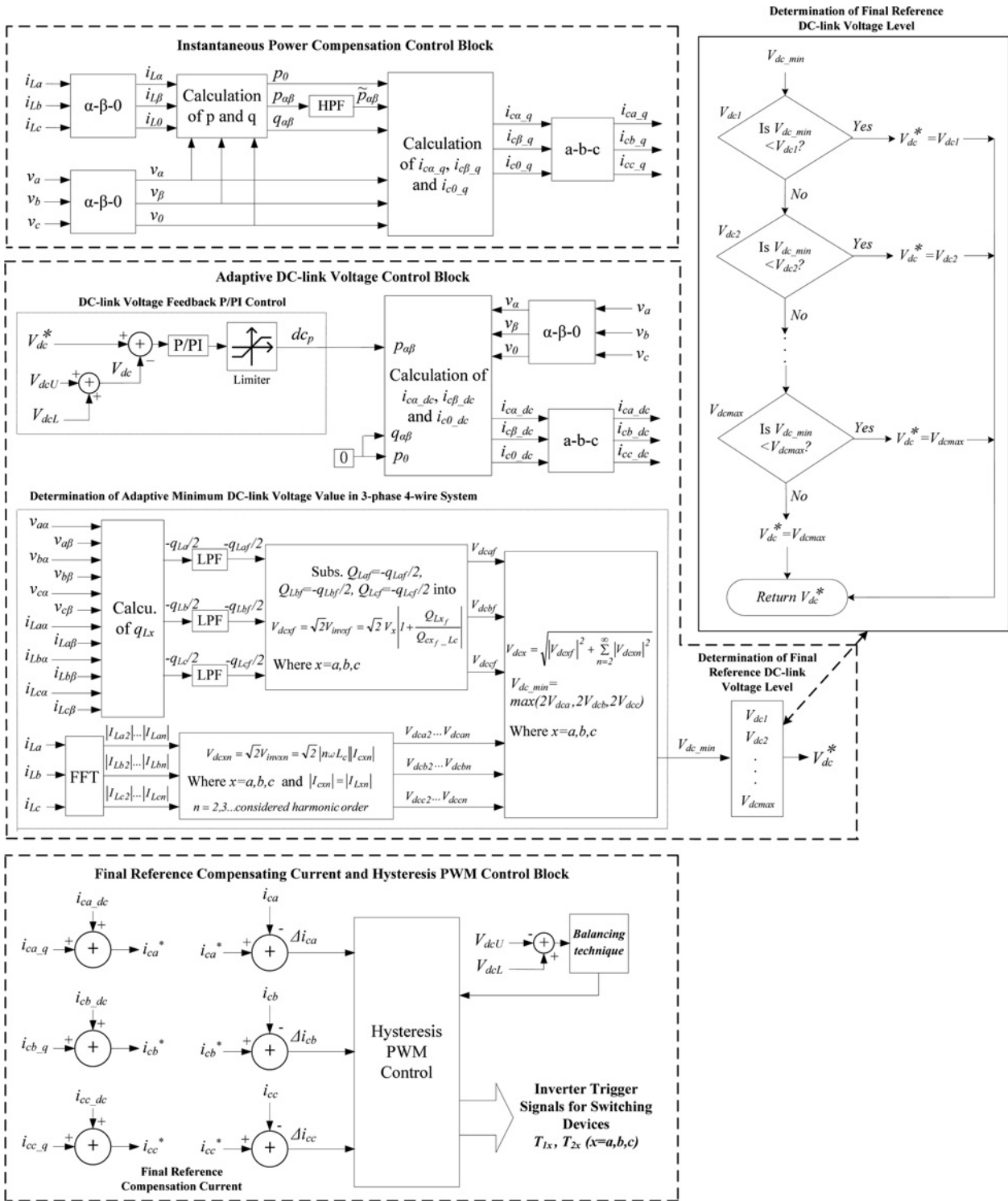


Fig. 3 Adaptive dc-link voltage control block diagram for APF

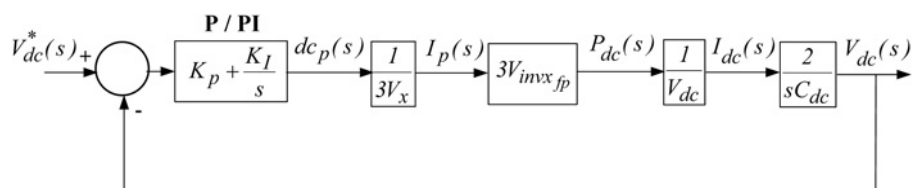


Fig. 4 Block diagram of APF dc-link voltage control

**Table 3** System and APF parameters for simulations and experiments

System parameters		Physical values
system voltage and frequency	$V_x, f$	110 V, 50 Hz
system inductance	$L_s$	0.5 mH
coupling inductance	$L_c$	30 mH
dc capacitor	$C_{dc}$	3.3 mF
dc-link voltage levels	$V_{dcU}, V_{dcL}$	200, 250, 300 V
first inductive non-linear loading	A, B, C $R_{NLx}, L_{NLx}$	50.0 $\Omega$ , 35.0 mH,
	$C_{NLx}$	400 $\mu$ F
second inductive linear loading	A, B, C $R_{LLx}, L_{LLx}$	15.0 $\Omega$ , 50.0 mH

close-loop transfer function can be expressed as

$$\frac{V_{dc}(s)}{V_{dc}^*(s)} = \frac{\frac{2V_{invx/p}K_p}{V_x V_{dc} C_{dc}} s + \frac{2V_{invx/p}K_I}{V_x V_{dc} C_{dc}}}{s^2 + \frac{2V_{invx/p}K_p}{V_x V_{dc} C_{dc}} s + \frac{2V_{invx/p}K_I}{V_x V_{dc} C_{dc}}} \quad (15)$$

By Routh–Hurwitz criterion, the Routh table for (15) can be obtained. As  $K_p$  and  $K_I > 0$ , the dc voltage controller is stable. From the APF system parameters in Table 3,  $L_c = 30$  mH,  $C_{dc} = 3.3$  mF and  $V_x = 110$  V. For the dc-link maximum operating voltage is  $V_{dcU}$ ,  $V_{dcL} = 300$  V, the fundamental compensating reactive current is  $|I_{cx_{fq}}| = 4.8$  A, when  $K_I = 50$ , the effect of  $K_p$  to the controller’s stability and dynamic response are shown in Figs. 5a and b. From Figs. 5a and b, when  $K_p$  is varying from 4 to 40, the phase margins are increasing from P.M.1 to P.M.2, which can improve the controllers’ stability. Moreover, a larger  $K_p$  value can also yield a faster dynamic response.

When only P controller is applied, that is  $K_I = 0$  in Fig. 4, the close-loop transfer functions can be deduced from (15). By Routh tables, as  $K_p > 0$ , the controller is stable. If  $K_p$  is selected too large, it yields a large fluctuation at steady state. On the other hand, if it is selected too small, a long settling time and a significant steady-state error will happen. In addition, the effect of  $K_p$  to the controller’s stability and dynamic response are shown in Figs. 5c and d. From Figs. 5c and d, when  $K_p$  is varying from 4 to 40, their phase margins (P.M.1 and P.M.2) do not change at all, and the controller obtain good stability. Moreover, a larger  $K_p$  value can yield a faster dynamic response.

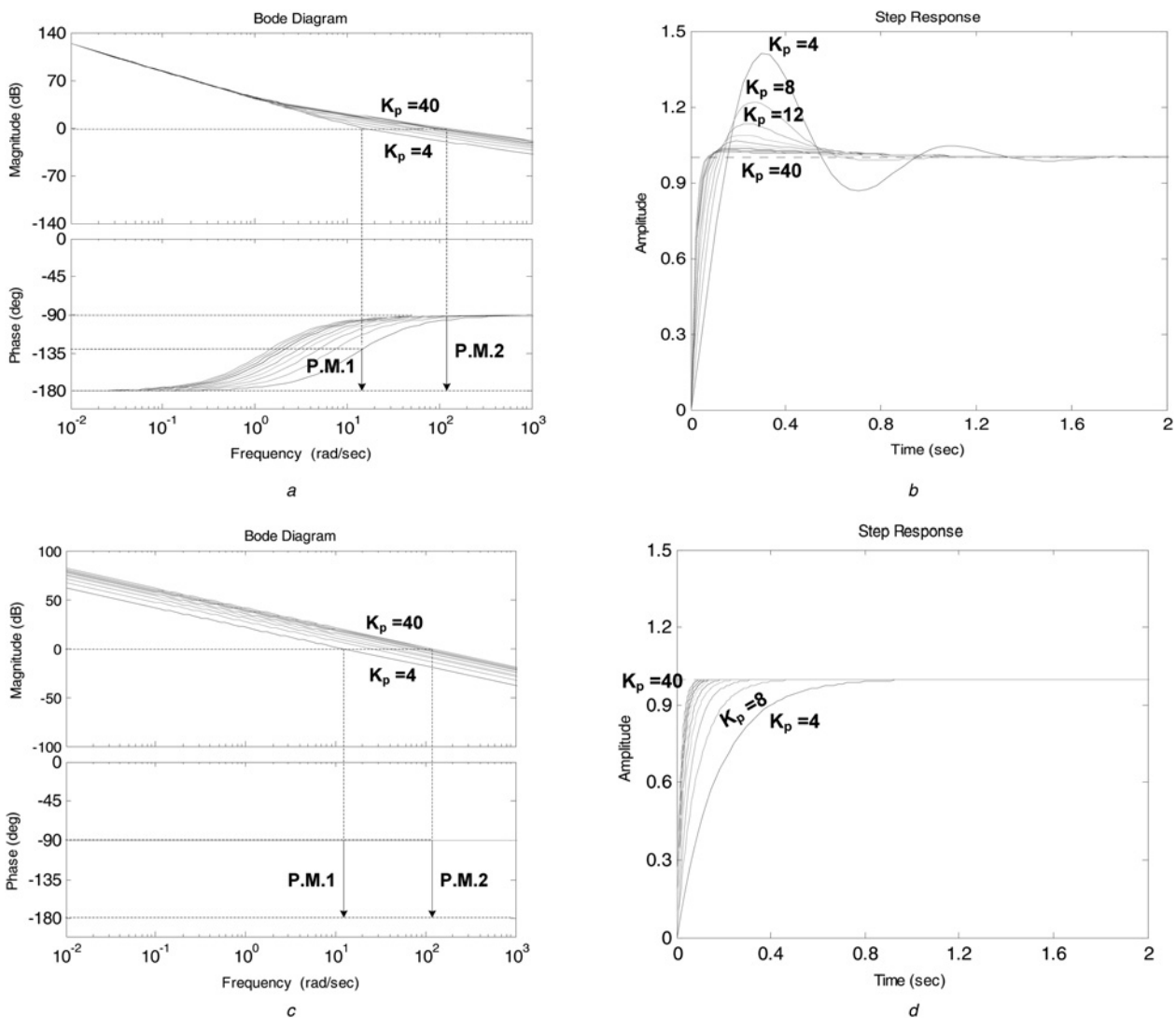
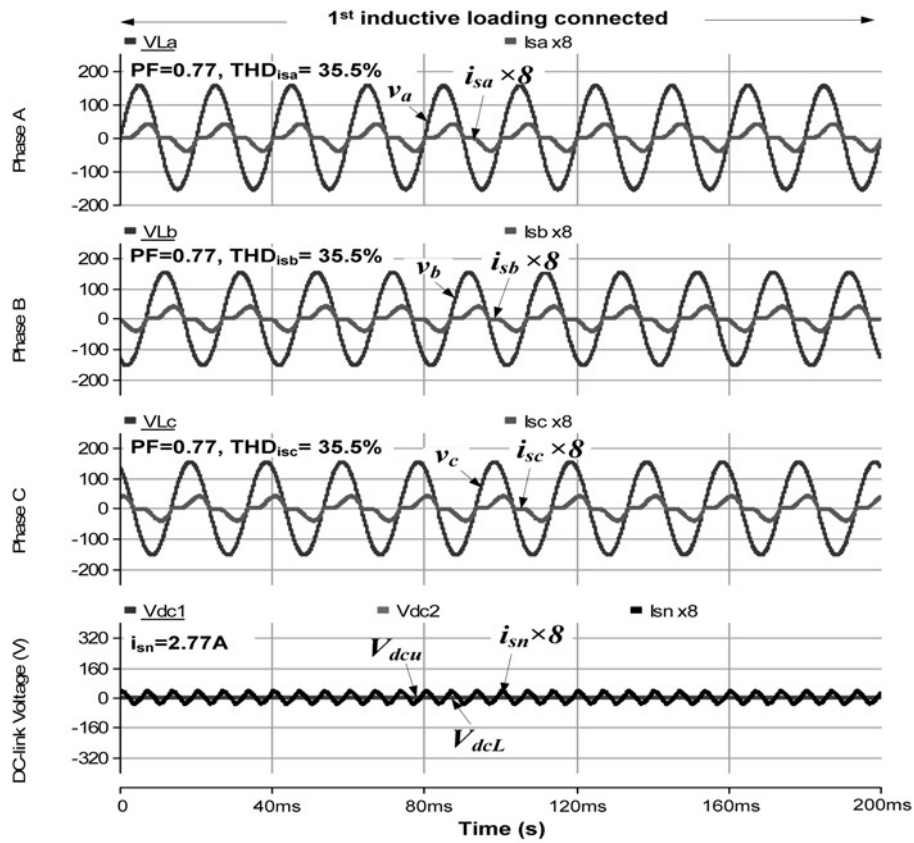
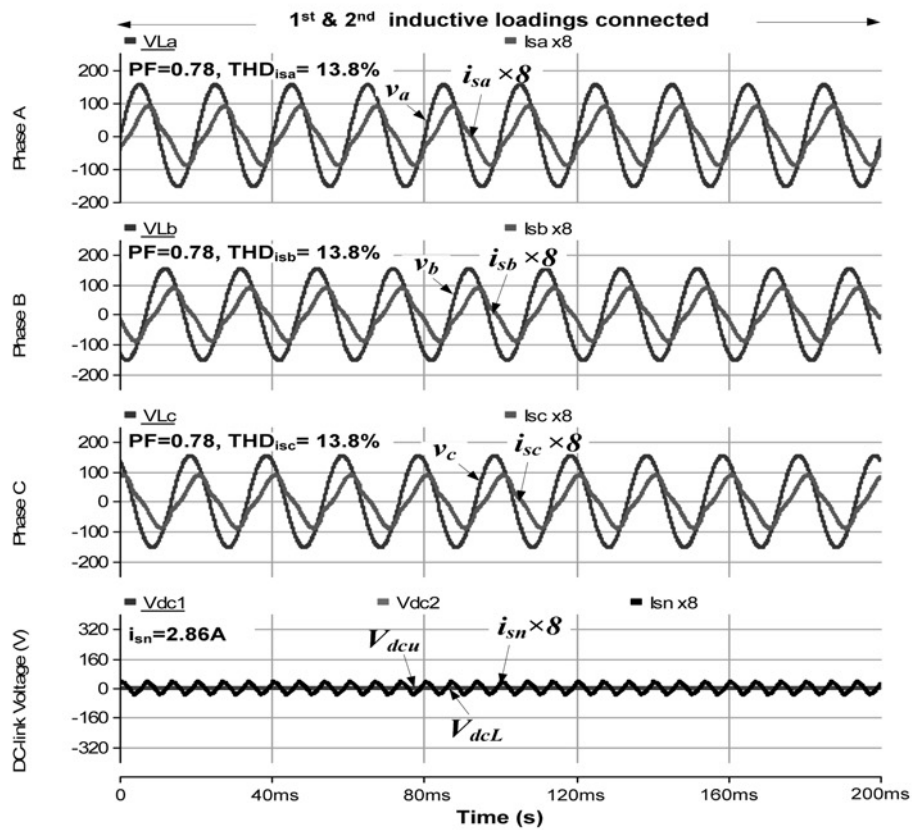


**Fig. 5** Stability and dynamic response of dc-link voltage feedback PI/P controller

- a Bode diagram with PI controller when  $K_I = 50$  and  $K_p$  varies from 4 to 40
- b Step response with PI controller when  $K_I = 50$  and  $K_p$  varies from 4 to 40
- c Bode diagram with P controller when  $K_p$  varies from 4 to 40
- d Step response with P controller when  $K_p$  varies from 4 to 40



a



b

**Fig. 6** Simulated and experimental PF, THD<sub>isx</sub> and *i<sub>sn</sub>* under different loading cases

- a Simulated PF, THD<sub>isx</sub> and *i<sub>sn</sub>* when first loading is connected
- b Simulated PF, THD<sub>isx</sub> and *i<sub>sn</sub>* when first and second loadings are connected
- c Experimental PF, THD<sub>isx</sub> and *i<sub>sn</sub>* when first loading is connected
- d Experimental PF, THD<sub>isx</sub> and *i<sub>sn</sub>* when first and second loadings are connected

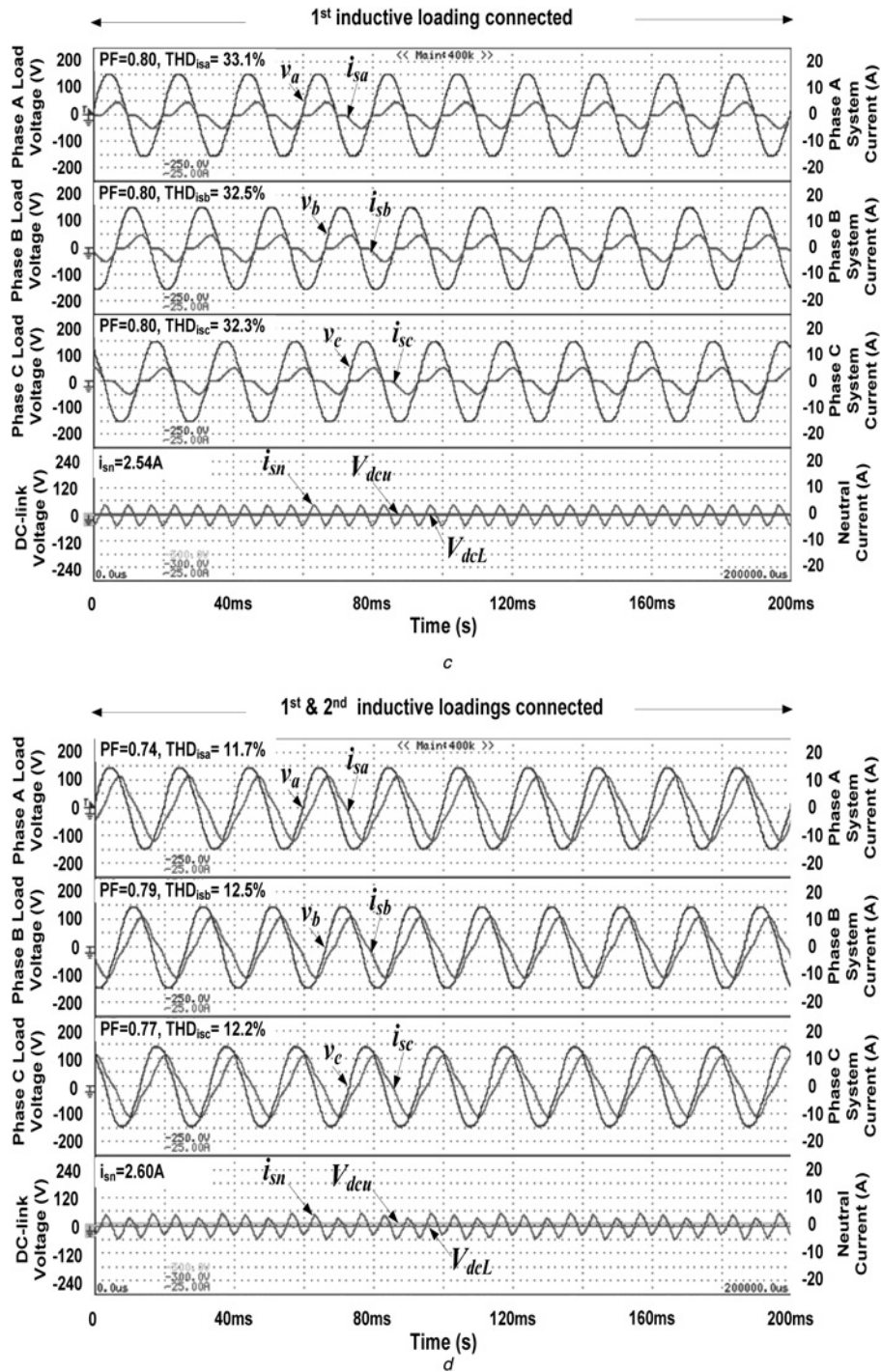


Fig. 6 Continued

In this paper, P controller is chosen because of its simplicity and memory resource saving in the digital signal processor (DSP). If zero steady-state error of dc control is appreciated, PI controller can be chosen. A limiter is also implemented to prevent the controller's overflow problem.

From [28], the three-phase instantaneous load voltages ( $v_a, v_b, v_c$ ) on the  $a-b-c$  coordinates can be transformed into those on the  $\alpha-\beta-0$  coordinates by the Clarke transformation

$$\begin{bmatrix} v_0 \\ v_\alpha \\ v_\beta \end{bmatrix} = \sqrt{\frac{2}{3}} \begin{bmatrix} 1/\sqrt{2} & 1/\sqrt{2} & 1/\sqrt{2} \\ 1 & -1/2 & -1/2 \\ 0 & \sqrt{3}/2 & -\sqrt{3}/2 \end{bmatrix} \begin{bmatrix} v_a \\ v_b \\ v_c \end{bmatrix} \quad (16)$$

The three-phase dc voltage control reference compensating currents in  $\alpha-\beta-0$  coordinates can be calculated via the following equation

$$\begin{bmatrix} i_{c0\_dc} \\ i_{c\alpha\_dc} \\ i_{c\beta\_dc} \end{bmatrix} = \frac{1}{v_{\alpha\beta}^2} \begin{bmatrix} v_{\alpha\beta}^2 & 0 & 0 \\ 0 & v_\alpha & -v_\beta \\ 0 & v_\beta & v_\alpha \end{bmatrix} \begin{bmatrix} 0 \\ dc_p \\ 0 \end{bmatrix} \quad (17)$$

where  $v_{\alpha\beta}^2 = v_\alpha^2 + v_\beta^2$ ,  $dc_p$  can be determined by (14). Finally, the three-phase dc voltage control reference compensating currents  $i_{c\alpha\_dc}$  in  $a-b-c$  coordinates can be obtained by the inverse matrix of Clarke transformation in  $\alpha-\beta-0$  coordinates, then  $V_{dc}$  can track



$V_{dc}^*$  by varying  $i_{cx\_dc}$

$$\begin{bmatrix} i_{ca\_dc} \\ i_{cb\_dc} \\ i_{cc\_dc} \end{bmatrix} = \sqrt{\frac{2}{3}} \begin{bmatrix} 1/\sqrt{2} & 1 & 0 \\ 1/\sqrt{2} & -1/2 & \sqrt{3}/2 \\ 1/\sqrt{2} & -1/2 & -\sqrt{3}/2 \end{bmatrix} \begin{bmatrix} i_{c0\_dc} \\ i_{c\alpha\_dc} \\ i_{c\beta\_dc} \end{bmatrix} \quad (18)$$

### 3.3 Final reference compensating current and hysteresis PWM control block

The hysteresis PWM [32] is applied for the PWM control part. After  $i_{cx\_q}$  and  $i_{cx\_dc}$  are calculated, the final reference compensating current  $i_{cx}^* = i_{cx\_q} + i_{cx\_dc}$ . After that,  $i_{cx}^*$  and  $i_{cx}$  will be sent to the hysteresis PWM control module for generating the corresponding PWM trigger signals to drive the power electronic switching devices. The dc capacitor voltage balancing concepts and techniques in [33] is also applied to balance the  $V_{dcU}$  and  $V_{dcL}$ .

## 4 Simulation and experimental results

Table 3 lists the system and APF parameters for simulations and experiments. As this paper mainly focuses on the APF application in low-voltage power distribution side, from [34], the inductance for a low-voltage distribution line is about 0.223 mH/km and the length of a low-voltage distribution line is usually no more than 1 km, thus its equivalent impedance is usually  $<0.1$  mH. In addition, during the APF experimental testing in the laboratory, a small rating coupling transformer is used to reduce grid voltage from 230 to 110 V. By considering them, the line inductance of the power distribution system of  $L_s = 0.5$  mH is put in the simulation study in this paper. In practical case, an 11 kV to 400 V transformer is applied in the distribution system, and the rating compared to our experimental platform is much larger, thus the impedance is much smaller to reduce the voltage drop across it. As discussed before,  $V_{dc}^*$  is pre-set into certain voltage levels ( $V_{dcU}$ ,  $V_{dcL} = 200, 250$  and 300 V) for preventing inverter dc voltage fluctuation phenomenon under the adaptive dc voltage control strategy. To simplify the verification, the three-phase loadings are balanced as illustrated in Fig. 6.

Simulations were carried out by using PSCAD/EMTDC. An 110 V, 5 kVA three-phase four-wire APF experimental prototype is designed and constructed in the laboratory. The digital control system of the APF is a DSP TMS320F2812. Moreover, the Mitsubishi IGBT intelligent power modules PM300DSA60 are employed as the switching devices of the inverter, and their switching frequency limitations are at 20 kHz. The sampling frequency of the control system is 25 kHz in both simulation and experiment. The hysteresis current PWM [32] is applied to achieve the compensating current tracking in this paper, in which the switching frequency is not fixed. The maximum switching frequency is 12.5 kHz, while the average switching frequency is around 4 kHz at fixed  $V_{dcU}$ ,  $V_{dcL} = 300$  V. From [35], it is suggested to select a coupling inductor  $L_c$  value close to the lower boundary because it could provide better current tracking speed with acceptable current ripples for APF. Thus, the coupling  $L_c$  of the APF can be designed via (19) [35], which is different from the design for HAPF based on one dominant current harmonic order [25, 26]

$$L_c \geq \frac{V_{dcmax}}{8f_{sw}\Delta I_{ripple}} \quad (19)$$

where  $V_{dcmax}$  is the maximum dc-link voltage,  $\Delta I_{ripple}$  is the maximum current ripple and  $f_{sw}$  is the switching frequency. For  $V_{dcmax} = 600$  V,  $\Delta I_{ripple} = 0.8$  A and the average  $f_{sw} = 4$  kHz, the coupling inductor  $L_c$  should be designed larger than 23.4 mH. Therefore,  $L_c$  is chosen to be 30 mH in this paper. In addition, this inductor value seems to be large because the capacity of the

**Table 4** APF minimum dc-link voltage levels (200, 250 and 300 V)

Different situations		Required $V_{dc\_min}/2$	Final minimum adapt. level $V_{dcU}$ , $V_{dcL}$
first loading	A, B, C	176 V	200 V
first and second loadings	A, B, C	210 V	250 V

testing APF system in the laboratory is small compared with those APF systems in the market [15–17]. If the current rating (capacity) of the APF increases, that means the allowable  $\Delta I_{ripple}$  is larger, and the required coupling  $L_c$  can be chosen as an appropriate small value accordingly (19), because the coupling  $L_c$  is inversely proportional to the current rating of the APF. In practical case, the capacity of the APF system is usually much larger than our experimental prototype, thus the coupling  $L_c$  for large capacity APF system will be usually much smaller than our case.

Fig. 6 shows the simulated and experimental PF, total harmonic distortion (THD<sub>isx</sub>) of  $i_{sx}$  and system neutral current ( $i_{sn}$ ) under different loading cases. When the first loading is connected, the three-phase simulated PF, THD<sub>isx</sub> and  $i_{sn}$  are 0.77, 35.5% and 2.77 A, respectively, while the three-phase experimental PF = 0.80, 0.80, 0.80, THD<sub>isx</sub> = 33.1, 32.5, 32.3% and  $i_{sn} = 2.54$  A, respectively. When first and second loadings are connected, the three-phase simulated PF, THD<sub>isx</sub> and  $i_{sn}$  are 0.78, 13.8% and 2.86 A, respectively, while the three-phase experimental PF = 0.74, 0.79, 0.77, THD<sub>isx</sub> = 11.7, 12.5, 12.2% and  $i_{sn} = 2.60$  A, respectively. Tables 5 and 8 illustrate the simulation and experimental results before APF compensation.

For the non-linear rectifier load as shown in Fig. 1, the most dominant harmonic current orders are third, fifth, seventh and ninth, respectively. To simplify the dc-link voltage calculation process in this paper, the required dc-link voltage for current harmonics compensation is calculated up to ninth-order only

**Table 5** Simulation results before APF compensation

Different cases		$Q_{sxf}$ (var)	PF	DPF	THD <sub>isx</sub> %	$i_{sxn}$ A
first loading	A, B, C	175	0.77	0.82	35.5	2.94
first and second loadings	A, B, C	487	0.78	0.79	13.8	7.19

**Table 6** Simulation results after APF compensation with adaptive dc voltage control strategy

Different cases		$Q_{sxf}$ (var)	PF	DPF	THD <sub>isx</sub> %	$i_{sxn}$ A	$V_{dcU}$ , $V_{dcL}$
first loading	A, B, C	-5	0.98	1.00	11.7	2.53	200 V
first and second loadings	A, B, C	-4	0.99	1.00	6.4	5.94	250 V

**Table 7** Simulation results after APF compensation with conventional fixed dc voltage control strategy

Different cases		$Q_{sxf}$ (var)	PF	DPF	THD <sub>isx</sub> %	$i_{sxn}$ A	$V_{dcU}$ , $V_{dcL}$
first loading	A, B, C	-7	0.96	1.00	12.3	2.85	300 V
first and second loadings	A, B, C	-2	0.99	1.00	6.9	6.11	300 V

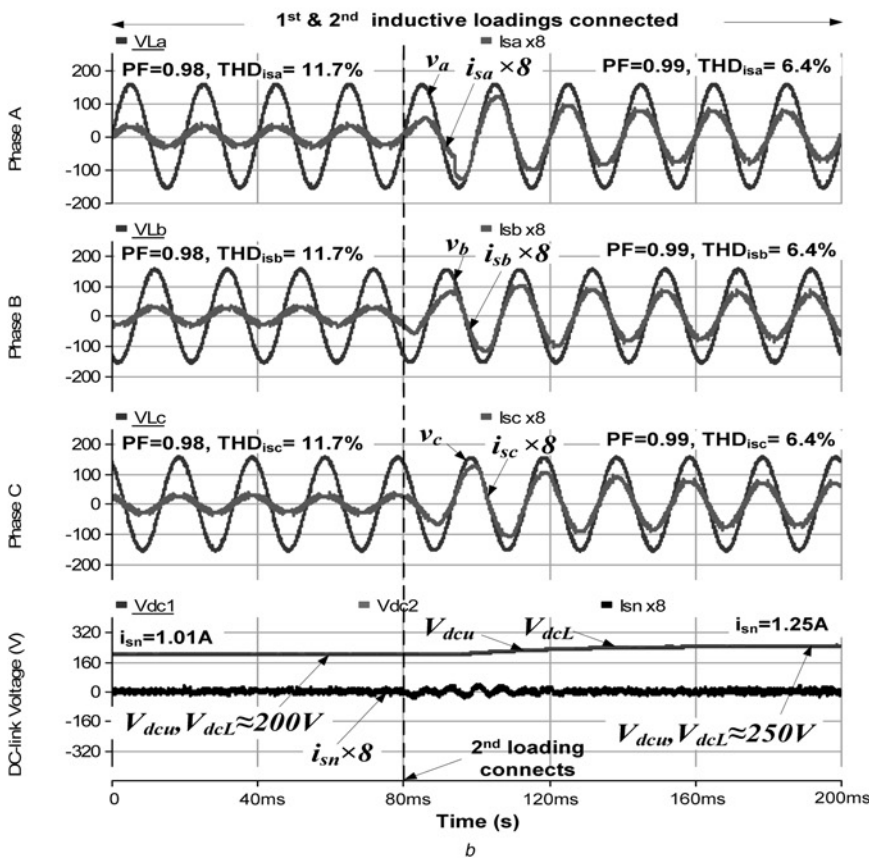
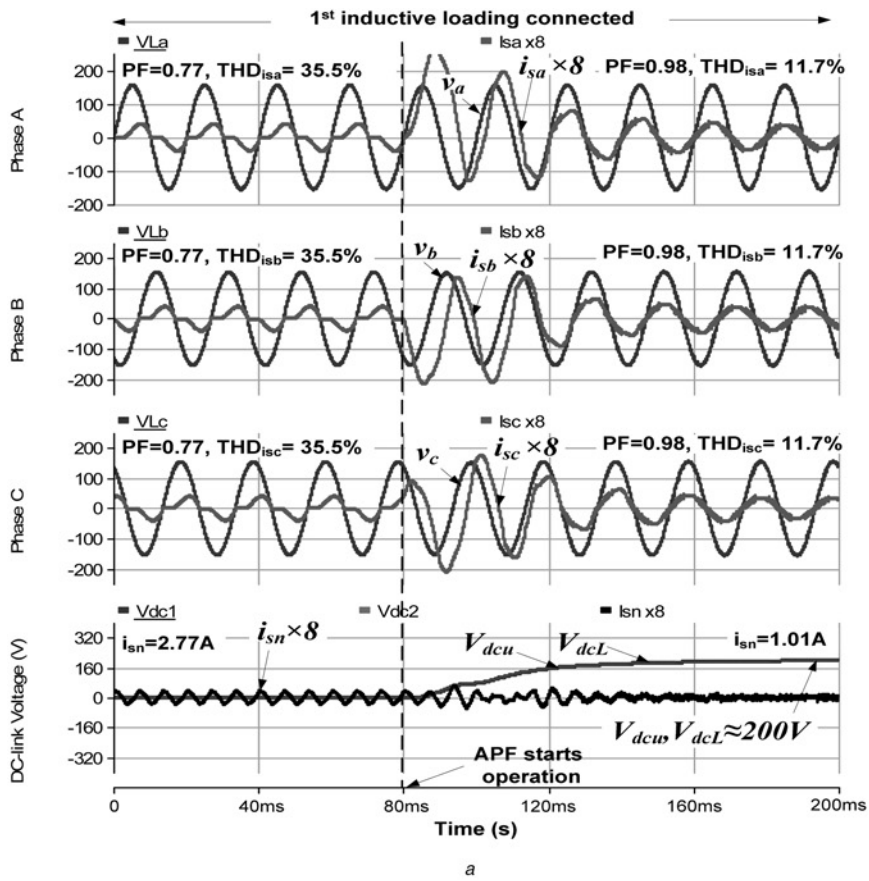


**Fig. 7** Dynamic compensation process of the APF in both simulation and experiment with adaptive dc voltage control  
 a Simulated PF, THD<sub>isx</sub>,  $i_{sn}$  and  $V_{dcU}$ ,  $V_{dcL}$  before and after APF starts operation during first loading  
 b Simulated PF, THD<sub>isx</sub>,  $i_{sn}$  and  $V_{dcU}$ ,  $V_{dcL}$  when second loading is connected  
 c Experimental PF, THD<sub>isx</sub>,  $i_{sn}$  and  $V_{dcU}$ ,  $V_{dcL}$  before and after APF starts operation during first loading  
 d Experimental PF, THD<sub>isx</sub>,  $i_{sn}$  and  $V_{dcU}$ ,  $V_{dcL}$  when second loading is connected

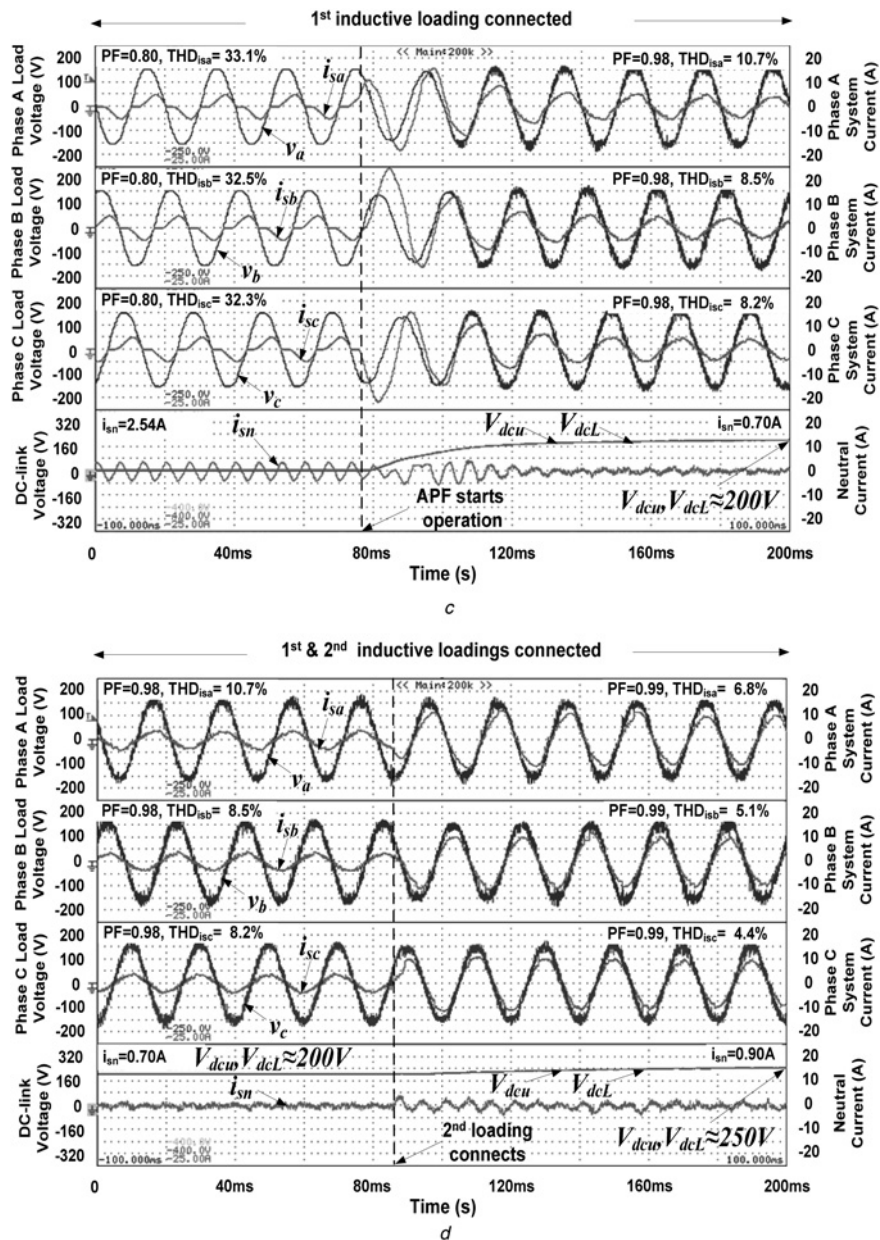


Fig. 7 Continued

because the load harmonic current contents beyond ninth-order are small. Of course, in general case, the required dc-link voltage can be calculated up to the considered load current harmonic order  $n$ . Refer to the pre-set voltage levels ( $V_{dcU}$ ,  $V_{dcL} = 200, 250$  and  $300$  V), from Table 4, the APF required minimum  $V_{dcU}$ ,  $V_{dcL} = 200$  and  $250$  V for compensating the first loading and first and second loadings. In addition, the power loss of APF can be calculated by measuring the collector–emitter voltage and current of each IGBT first, then the total inverter power loss  $P_{loss}$  can be found through the following equation [36]

$$P_{loss} = \sum_{n=0}^{n=6} P_{loss,n} = \sum_{n=0}^{n=6} \frac{1}{t_f} \int_0^{t_f} v_{ce,n}(t) \cdot i_{ce,n}(t) dt \quad (20)$$

where  $v_{ce,n}(t)$  and  $i_{ce,n}(t)$  are the collector–emitter voltage and current of IGBT, respectively.  $t_f$  is a fundamental period and  $n$  is the number of IGBT. In the following, simulation and experimental results for the proposed control strategy will be presented in comparison with the conventional fixed dc voltage control.

#### 4.1 Compensation results with adaptive dc voltage controlled APF

After compensated by the APF with adaptive dc voltage control strategy, the dynamic compensation process of the APF in both simulation and experiment are shown in Fig. 7, and the overall compensation results are listed in Tables 6 and 9. From Fig. 7, it can be observed that the dc-link voltage is adaptively controlled to different levels according to different loading conditions. The simulated and experimental PF, THD<sub>isx</sub> and  $i_{sn}$  can be improved to 0.98 or above, within 12% and significantly reduced after APF compensation for both loadings case, compared with Fig. 6. Moreover, the system current  $i_{sx}$  is significantly reduced after the APF compensation.

#### 4.2 Comparison between fixed and adaptive dc-link voltage control

After compensated by the APF with fixed  $V_{dcU}$ ,  $V_{dcL} = 300$  V, the dynamic compensation process of the APF in both simulation and experiment are shown in Fig. 8, and the overall compensation

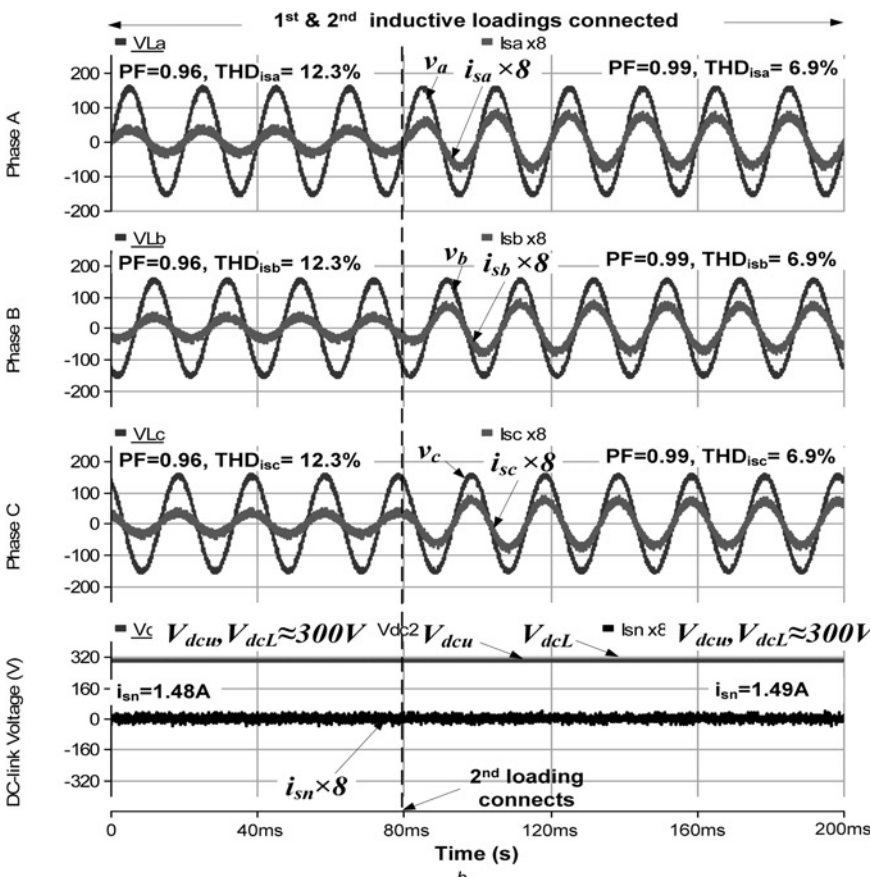
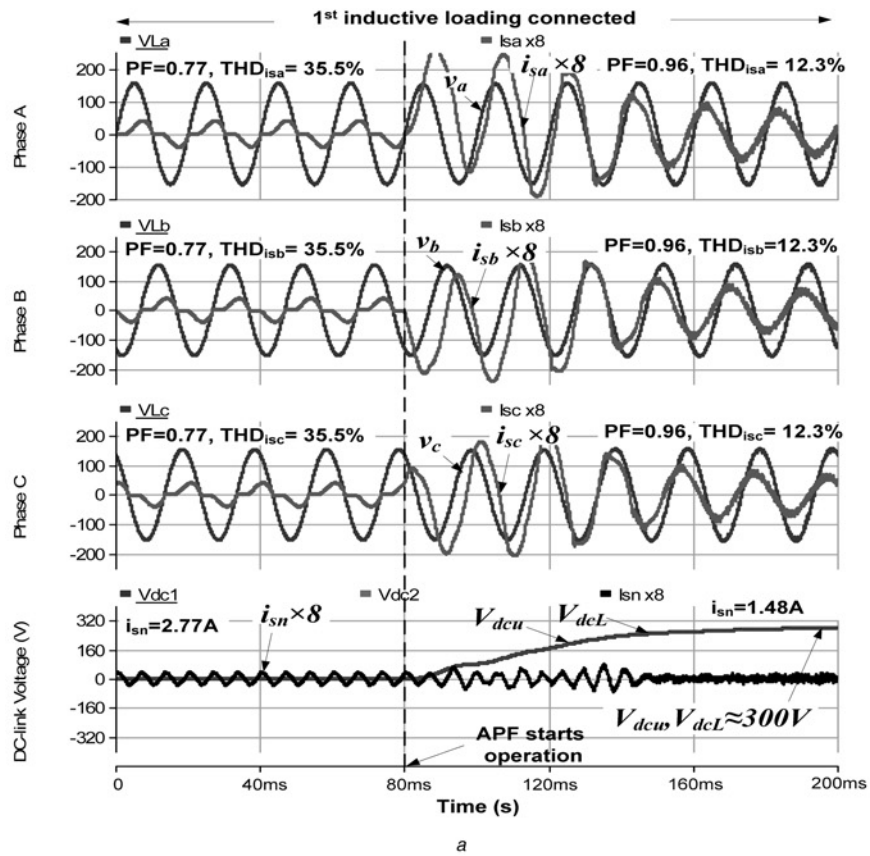


**Fig. 8** Dynamic compensation process of the APF in both simulation and experiment with fixed  $V_{dcU}$ ,  $V_{dcL} = 300\text{ V}$

- a Simulated PF, THD<sub>iscs</sub>,  $i_{sn}$  and  $V_{dcU}$ ,  $V_{dcL}$  before and after APF starts operation during first loading
- b Simulated PF, THD<sub>iscs</sub>,  $i_{sn}$  and  $V_{dcU}$ ,  $V_{dcL}$  when second loading is connected
- c Experimental PF, THD<sub>iscs</sub>,  $i_{sn}$  and  $V_{dcU}$ ,  $V_{dcL}$  before and after APF starts operation during first loading
- d Experimental PF, THD<sub>iscs</sub>,  $i_{sn}$  and  $V_{dcU}$ ,  $V_{dcL}$  when second loading is connected

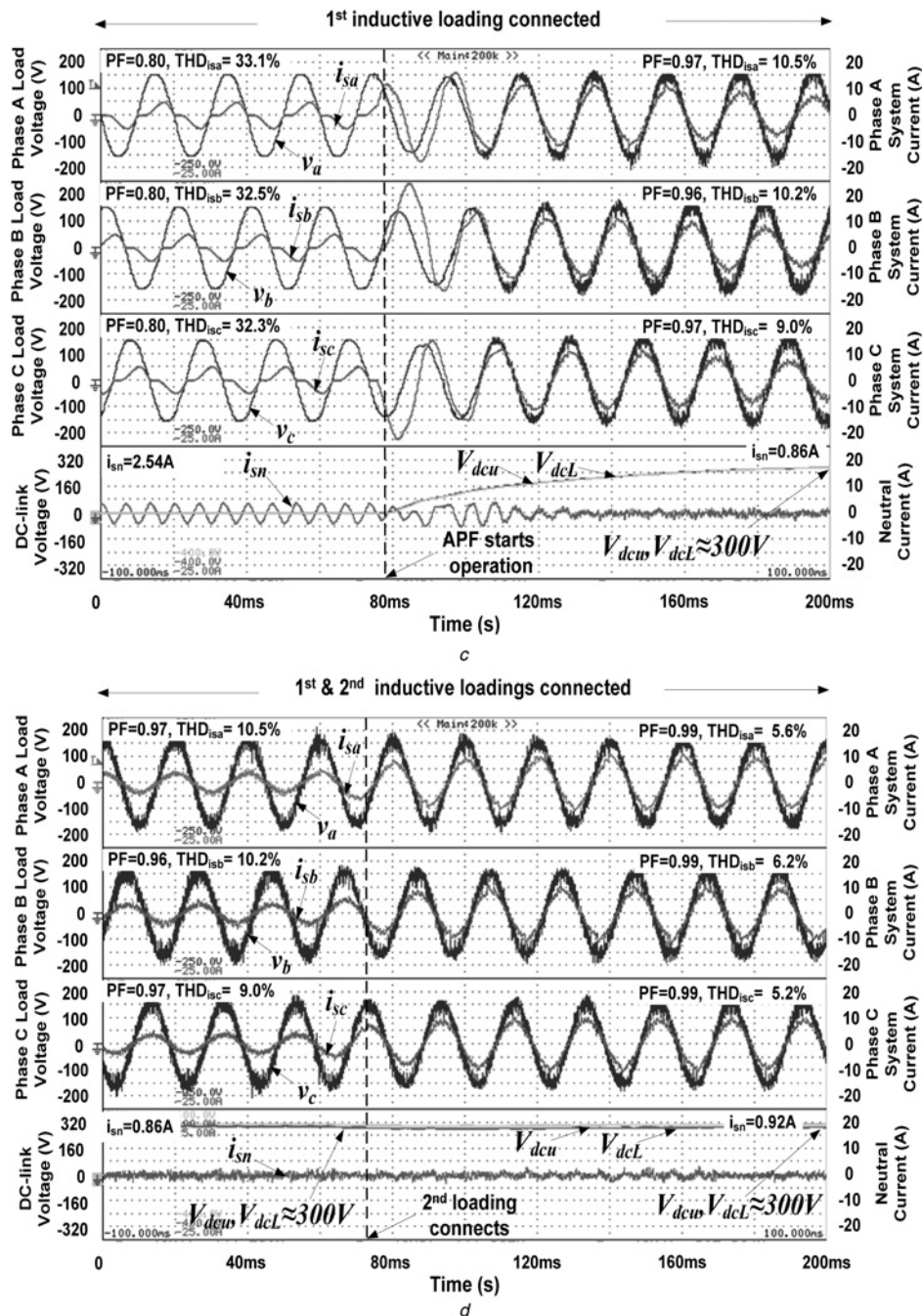


Fig. 8 Continued

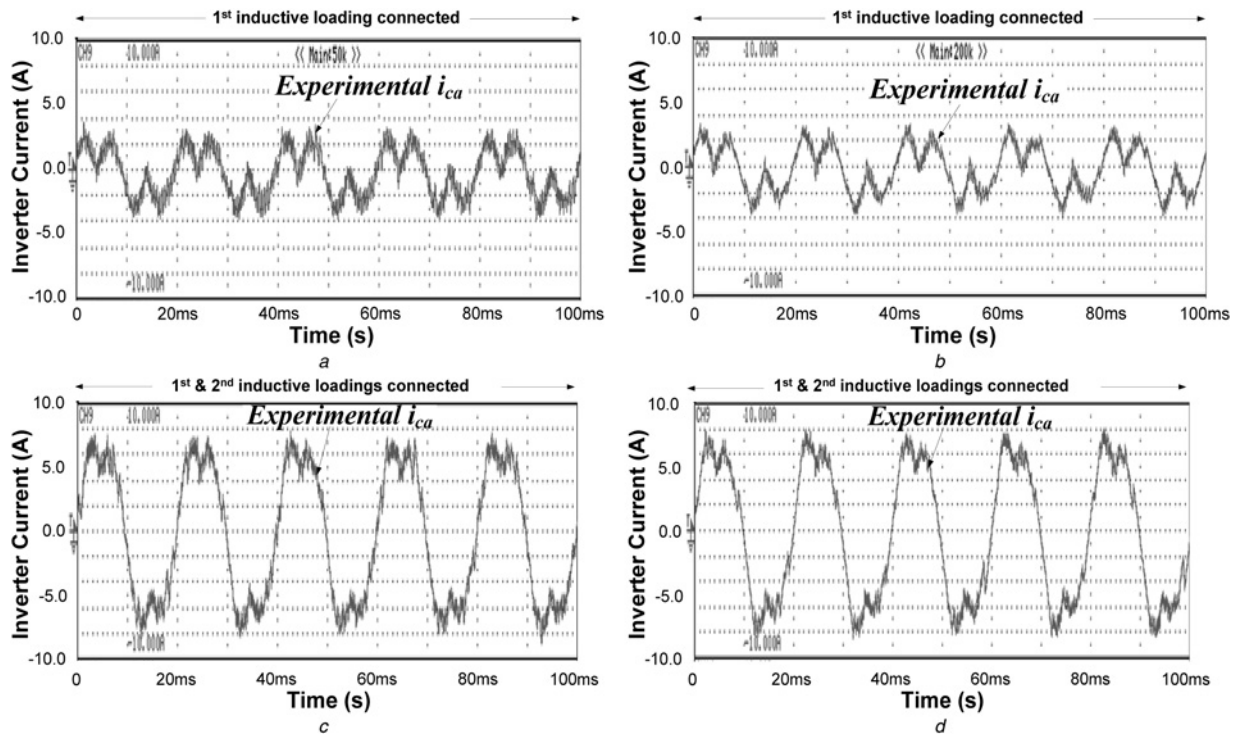
results are listed in Tables 7 and 10. Compared Fig. 8 with Fig. 7 as well as Tables 7 and 10 with Tables 6 and 9, the fixed and adaptive dc voltage control can obtain almost the same steady-state compensation results. However, the proposed control strategy solely requires lower dc voltage levels for compensating the first loading and the first together with the second loadings as shown in Figs. 7 and 8. Thus, it obtains less  $THD_{i_{sx}}$ ,  $i_{sn}$  and  $i_{sx}$  values for both loading cases, because a lower dc-link voltage will generate less switching noise into the system, and vice versa. For the proposed control strategy, due to its final reference  $V_{dc}^*$  is varying at different loading cases, the compensating performance is affected at each  $V_{dc}$  varying. Compared with the conventional one, the adaptive one obtains a longer settling time during both the loading and  $V_{dc}$  level varying case. Moreover, its dynamic response will be sacrificed a little bit under an adaptive low dc operating voltage.

Fig. 9 shows the APF experimental compensating current  $i_{cx}$  of phase  $a$  with: (a) fixed  $V_{dcU}$ ,  $V_{dcL} = 300$  V control and (b) adaptive

dc voltage control during the first loading connected case, (c) fixed  $V_{dcU}$ ,  $V_{dcL} = 300$  V control and (d) adaptive dc voltage control during the first together with the second loadings connected case. Fig. 9 shows that the proposed adaptive control strategy can effectively lower the switching noise of the APF in comparison to

Table 8 Experimental results before APF compensation

Different cases		$Q_{sxf}$ (var)	PF	DPF	$THD_{i_{sxf}}$ %	$i_{sxf}$ A
first loading	A	191	0.80	0.85	33.1	2.83
	B	192	0.80	0.85	32.5	2.88
	C	187	0.80	0.85	32.3	2.84
first and second loadings	A	530	0.74	0.76	11.7	7.45
	B	450	0.79	0.80	12.5	7.02
	C	460	0.77	0.79	12.2	7.04



**Fig. 9** Experimental  $i_{ca}$  of phase a with

- a Fixed  $V_{dcU}$ ,  $V_{dcL} = 300$  V control during first loading connected case
- b Adaptive dc-link voltage control during first loading connected case
- c Fixed  $V_{dcU}$ ,  $V_{dcL} = 300$  V control during first and second loadings connected case
- d Adaptive dc-link voltage control during first and second loadings connected case

**Table 9** Experimental results after APF compensation with adaptive dc voltage control strategy

Different cases		$Q_{sxf}$ (var)	PF	DPF	THD <sub><math>i_{sxr}</math></sub> %	$i_{sxr}$ A	$V_{dcU}$ , $V_{dcL}$
first loading	A	51	0.98	1.00	10.7	2.46	200 V
	B	52	0.98	1.00	8.5	2.39	
	C	48	0.98	1.00	8.2	2.45	
first and second loadings	A	80	0.99	1.00	6.8	6.01	250 V
	B	100	0.99	1.00	5.1	5.90	
	C	80	0.99	1.00	4.4	6.02	

**Table 10** Experimental results after APF compensation with conventional fixed dc voltage control strategy

Different cases		$Q_{sxf}$ (var)	PF	DPF	THD <sub><math>i_{sxr}</math></sub> %	$i_{sxr}$ A	$V_{dcU}$ , $V_{dcL}$
first loading	A	70	0.97	1.00	10.5	2.53	300 V
	B	78	0.96	1.00	10.2	2.57	
	C	71	0.97	1.00	9.0	2.57	
first and second loadings	A	100	0.99	1.00	5.6	6.11	300 V
	B	120	0.99	1.00	6.2	6.17	
	C	110	0.99	1.00	5.2	6.17	

**Table 11** Experimental inverter power loss of APF with fixed  $V_{dcU}$ ,  $V_{dcL} = 300$  V and adaptive dc voltage control

Inverter power loss of APF		Fixed $V_{dcU}$ , $V_{dcL} = 300$ V	Adaptive dc
power loss, W	first loading	186.6 W	118.2 W (200 V) ~37% decrease
	first and second loadings	368.4 W	223.2 W (250 V) ~39% decrease

the conventional fixed  $V_{dcU}$ ,  $V_{dcL} = 300$  V operation. Moreover, from Table 11, the adaptive control strategy can reduce the inverter power loss by 37 and 39%, respectively, compared with the conventional fixed  $V_{dcU}$ ,  $V_{dcL} = 300$  V control. From Table 11, this adaptive dc control technique should be more effective in APF application because it requires a high dc-link operating voltage compared with that of HAPF. Thus, the switching-loss reduction for APF will be more significant.

From Figs. 6–9 and Tables 5–11, they verified that the proposed control strategy can significantly reduce the APF operational switching loss and switching noise and improve its compensation results without adding-in any soft-switching circuit.

The capacity of the testing APF system in this paper is small due to the laboratory facilities' limitations. As the reference compensating current in steady state is the same for both conventional fixed and proposed adaptive dc-link voltage controlled APFs, the compensating current should be approximately the same. Thus, the inverter power loss reduction (efficiency enhancement) is mainly due to the dc-link voltage reduction. In addition, if the capacity (compensating current rating) of the APF system is larger, the trend of the power loss reduction still maintains because the difference between their inverter power losses is mainly due to the difference between their dc-link voltage levels.

In addition, as this paper focuses on the APF application in low-voltage power distribution side, the neutral wire presents, thus the proposed adaptive dc-link voltage control strategy for three-phase four-wire APF works even if the load is not connecting to the neutral point, such as: a three-phase ac to dc rectifier load or the load is in delta connection. Moreover, even though the change of the three-phase loadings may not be identical, the proposed controlled APF can still compensate the reactive power and current harmonics problems. At the same time, the adaptive dc-link voltage control strategy can reduce the inverter part switching loss and switching noise in comparison with the conventional fixed dc-link voltage control.

## 5 Conclusion

Soft-switching techniques are usually applied to reduce the operating switching loss of the high dc voltage controlled APF. However, they all require extra auxiliary circuits, thus increasing the system initial cost. To obtain loss reduction function without adding extra circuit components, an adaptive dc voltage control strategy for APF is proposed. The dc voltage controller's design criteria including the stability study and dynamic performance analysis are discussed. In addition, the viability of the proposed controller for APF in lowering switching loss and switching noise is verified by both simulation and experimental results, compared with the traditional fixed dc voltage controlled APF and the APF with soft-switching auxiliary circuits.

## 6 Acknowledgement

This work is supported by the Macao Science and Technology Development Fund (FDCT) (FDCT 109/2013/A3) and the Research Committee of University of Macau (MRG012/WMC/2015/FST, MYRG2015-00030-AMSV and SRG2014-00007-AMSV).

## 7 References

- 1 Trinh, Q.-N., Lee, H.-H.: 'An advanced current control strategy for three-phase shunt active power filters', *IEEE Trans. Ind. Electron.*, 2013, **60**, (12), pp. 5400–5410
- 2 Senini, S.T., Wolfs, P.J.: 'Systematic identification and review of hybrid active filter topologies'. Proc. of IEEE 33rd Annual Power Electronics Specialists Conf., PESC. 02, 2002, vol. 1, pp. 394–399
- 3 Rahmani, S., Mendalek, N., Al-Haddad, K.: 'Experimental design of a nonlinear control technique for three-phase shunt active power filter', *IEEE Trans. Ind. Electron.*, 2013, **57**, (10), pp. 3364–3375
- 4 Garcia-Cerrada, A., Pinzon-Ardila, O., Feliu-Batlle, V., *et al.*: 'Application of a repetitive controller for a three-phase active power filter', *IEEE Trans. Power Electron.*, 2007, **22**, (1), pp. 237–246
- 5 Chauhan, S.K., Shah, M.C., Tiwari, R.R., *et al.*: 'Analysis, design and digital implementation of a shunt active power filter with different schemes of reference current generation', *IET Power Electron.*, 2014, **7**, (3), pp. 627–639
- 6 Suresh, Y., Panda, A.K., Suresh, M.: 'Real-time implementation of adaptive fuzzy hysteresis-band current control technique for shunt active power filter', *IET Power Electron.*, 2012, **5**, (7), pp. 1188–1195
- 7 Xiao, Z., Deng, X., Yuan, R., *et al.*: 'Shunt active power filter with enhanced dynamic performance using novel control strategy', *IET Power Electron.*, 2014, **7**, (12), pp. 3169–3181
- 8 Garcia Campanhol, L.B., Oliveira da Silva, S.A., Goedtel, A.: 'Application of shunt active power filter for harmonic reduction and reactive power compensation in three-phase four-wire systems', *IET Power Electron.*, 2014, **7**, (11), pp. 2825–2836
- 9 Gomez Jorge, S., Busada, C.A., Solsona, J.: 'Reduced order generalised integrator-based current controller applied to shunt active power filters', *IET Power Electron.*, 2014, **7**, (5), pp. 1083–1091
- 10 Kanjiya, P., Khadkikar, V., Zeineldin, H.H.: 'A noniterative optimized algorithm for shunt active power filter under distorted and unbalanced supply voltages', *IEEE Trans. Ind. Electron.*, 2013, **60**, (12), pp. 5376–5390
- 11 de Araujo Ribeiro, R.L., de Azevedo, C.C., de Sousa, R.M.: 'A robust adaptive control strategy of active power filters for power-factor correction, harmonic compensation, and balancing of nonlinear loads', *IEEE Trans. Power Electron.*, 2012, **27**, (2), pp. 718–730
- 12 Akagi, H.: 'New trends in active filters for power conditioning', *IEEE Trans. Ind. Appl.*, 1996, **32**, (6), pp. 1312–1322
- 13 Akagi, H.: 'Modern active filters and traditional passive filters', *Bull. Pol. Acad. Sci. Tech. Sci.*, 2006, **54**, (3), pp. 255–269
- 14 Asiminoaei, L., Rodriguez, P., Blaabjerg, F., *et al.*: 'Reduction of switching losses in active power filters with a new generalized discontinuous-PWM strategy', *IEEE Trans. Ind. Electron.*, 2008, **55**, (1), pp. 467–471
- 15 Specification of Honeywell SmartWave APF. Available at [http://www.honeywell-powercontrol.com/English/Product\\_APF.aspx#](http://www.honeywell-powercontrol.com/English/Product_APF.aspx#)
- 16 Specification of ABB Power Quality Filters PQFI-PQFM-PQFS. Available at <http://www.abb.com/product/seitp329/e83ed739e0daa5a9c1256f85004e548b.aspx?productLanguage=us&country=00>
- 17 Specification of INJET APF. Available at <http://www.injet.cn/en/content/?338.html>
- 18 Chang, J., Hu, J.: 'Modular design of soft-switching circuits for two-level and three-level inverters', *IEEE Trans. Power Electron.*, 2006, **21**, (1), pp. 131–139
- 19 Divan, D.M., Venkataramanan, G., DeDoncker, R.W.A.A.: 'Design methodologies for soft switched inverters', *IEEE Trans. Ind. Appl.*, 1993, **29**, (1), pp. 126–135
- 20 De Doncker, R.W., Lyons, J.P.: 'The auxiliary resonant commutated pole converter'. Conf. Record of IEEE Industry Applications Society Annual Meeting, October 1990, vol. 2, pp. 1228–1235
- 21 Asiminoaei, L., Blaabjerg, F., Hansen, S., *et al.*: 'Adaptive compensation of reactive power with shunt active power filters', *IEEE Trans. Ind. Appl.*, 2008, **44**, (3), pp. 867–877
- 22 Wong, M.-C., Tang, J., Han, Y.-D.: 'Cylindrical coordinate control of three-dimensional PWM technique in three-phase four-wired trilevel inverter', *IEEE Trans. Power Electron.*, 2003, **18**, pp. 208–220
- 23 Lao, K.-W., Dai, N.-Y., Liu, W.-G., *et al.*: 'Hybrid power quality compensator with minimum dc operation voltage design for high-speed traction power systems', *IEEE Trans. Power Electron.*, 2013, **28**, (4), pp. 2024–2036
- 24 Lam, C.-S., Choi, W.-H., Wong, M.-C., *et al.*: 'Adaptive dc-link voltage controlled hybrid active power filters for reactive power compensation', *IEEE Trans. Power Electron.*, 2012, **27**, (4), pp. 1758–1772
- 25 Lam, C.-S., Cui, X.-X., Choi, W.-H., *et al.*: 'Minimum inverter capacity design for three-phase four-wire LC-hybrid active power filters', *IET Power Electron.*, 2012, **5**, (7), pp. 956–968
- 26 Lam, C.-S., Wong, M.-C., Choi, W.-H., *et al.*: 'Design and performance of an adaptive low-dc-voltage-controlled LC-hybrid active power filter with a neutral inductor in three-phase four-wire power systems', *IEEE Trans. Ind. Electron.*, 2014, **61**, (6), pp. 2635–2647
- 27 Lam, C.-S., Cui, X.-X., Wong, M.-C., *et al.*: 'Minimum DC-link voltage design of three-phase four-wire active power filters'. IEEE 13th Workshop on Control and Modeling for Power Electronics (COMPEL), 2012, June 2012
- 28 Akagi, H., Ogasawara, S., Hyosung, K.: 'The theory of instantaneous power in three-phase four-wire systems: a comprehensive approach'. Conf. Record of the IEEE-34th IAS Annual Meeting, 1999, vol. 1, pp. 431–439
- 29 Khadkikar, V., Chandra, A., Singh, B.N.: 'Generalized single-phase p-q theory for active power filtering: simulation and DSP-based experimental investigation', *IET Power Electron.*, 2009, **2**, (1), pp. 67–78
- 30 Wu, L.H., Zhuo, F., Zhang, P.B., *et al.*: 'Study on the influence of supply-voltage fluctuation on shunt active power filter', *IEEE Trans. Power Deliv.*, 2007, **22**, pp. 1743–1749
- 31 Choi, W.-H., Lam, C.-S., Wong, M.-C., *et al.*: 'Analysis of dc-link voltage controls in three-phase four-wire hybrid active power filters', *IEEE Trans. Power Electron.*, 2013, **28**, (5), pp. 2180–2191
- 32 Lam, C.-S., Wong, M.-C., Han, Y.-D.: 'Hysteresis current control of hybrid active power filters', *IET Power Electron.*, 2012, **5**, (7), pp. 1188–1195
- 33 Aredes, M., Hafner, J., Heumann, K.: 'Three-phase four-wire shunt active filter control strategies', *IEEE Trans. Power Electron.*, 1997, **12**, pp. 311–318
- 34 Studio of Electricians: 'Electrician common data handbook' (Shanghai Science and Technology Press, 2013), ISBN 9787547816646
- 35 Dai, N.-Y., Wong, M.-C.: 'Design considerations of coupling inductance for active power filters'. The 6th IEEE Conf. on Industrial Electronics and Applications (ICIEA2011), Beijing, China, June 2011, pp. 1370–1375
- 36 Xiao, C., Chen, G., Odendaal, W.G.: 'Overview of power loss measurement techniques in power electronics systems', *IEEE Trans. Ind. Appl.*, 2007, **43**, (3), pp. 657–664